

## Shock Structural Tests for NSRR Experimental Capsule Using Slow Explosive (II)

Shinji YOSHIE, Morihiko IWASAKI  
*Kawasaki Heavy Industries Ltd., Tokyo, Japan*

Sadamitsu TANZAWA, Toshio FUJISHIRO  
*Japan Atomic Energy Research Institute, Tokaimura, Japan*

### ABSTRACT

The present study was conducted to experimentally understand the shock structural characteristics of a cylindrical capsule used for failure tests of Light Water Reactor fuel rods. This paper describes the dynamic correlation between pressure waves in fluid and the plastic deformation of a capsule that interact with each other.

### 1. INTRODUCTION

Following the previous report (I) (Tanzawa et al. 1989), this paper shows the shock structural characteristics of a capsule used in the Nuclear Safety Research Reactor (NSRR). The authors have been conducting out-pile tests where slow explosives are used to simulate impulsive pressure in coolant (water) generated at the time of fuel rod failure in the Reactivity Initiated Accident (RIA). The previous report discussed the pressure wave propagation behavior and the basic fluid-structure interaction in a capsule with comparatively higher rigidity, which did not deform plastically near a source part.

On the basis of the latest tests where the shell thickness of a capsule and the energetics level of source were used as parameters, this paper presents dynamic correlation between energetics level and absorbed strain energy of a capsule.

### 2. EXPERIMENTAL PROCEDURE AND PARAMETERS

The capsule structure is shown in Figure 1. Two pressure transducers (100 MPa max.; allowable overload: 150%) and eighteen strain gages (max. plastic strain: 10%) were attached to the capsule made of the stainless steel type 304. Figure 2 shows the nominal stress-strain curve obtained when uni-axial tension was applied up to the strain rate  $\dot{\epsilon} = 2 \text{ sec}^{-1}$ . The thicknesses of a capsule with an identical inner diameter are 1.5, 2 and 3 mm. The levels of initial peak pressure of the source are set at 40 and 60 Mpa. Based on the Mises equivalent stress, 40 MPa is set as a reference level which is enough to make the 3 mm thick capsule shell yield. The duration of pressure waves near the source was fixed in all tests at about 1 ms including the radial reflection.

### 3. ENERGY CALIBRATION

The kinetic energy of the water column (slug) above the explosive will provide an index for the discussion of slug impact pressure or the deformation of the upper part of a capsule. Therefore, as was described in the previous report, a float was put on the water surface to examine the velocity history. To find the released energy history of the source in the present study, an acrylic cylinder shown in Figure 3 was made to directly catch the expansion history of combustion gas with a high-speed camera.

Photos of gas expansion with a 40 MPa source are shown in Figure 4. Figure 5 shows the comparison between the direct observation of gas expansion and the movement of a float. When a float was used, the initial rise was delayed due to the inertia and the compressibility of the float. In this case, the gas expansion history may also be estimated by artificially moving the starting point to the 0 point. Figure 6 illustrates pressure and gas work-volume change relationships when a 40 MPa source was used.

For estimation of the energy shock wave using the pressure history  $P(t)$  near the source, the gas work done  $W$  (Cole 1965) without afterflow is denoted by  $W(R) = (4\pi R^2 / \rho_0 C_0) \int_{t(R)}^{\tau} P^2 dt$ . Then the PI value defined by the following are presupposed on the basis of the above formula and was compared with the gas work computed by integral  $\int_0^{V_c} P dV$  ( $V_c$ : cover-gas volume).

$$PI = \frac{4\pi R^2}{\rho C} Pp \cdot I, \quad I = \int_0^{t'} P dt$$

where

- R : shock front radius
- $Pp$  : initial peak pressure near the source
- P : pressure history near the source
- I : impulse of unit area
- $t'$  : duration time of pressure
- $\rho$  : density of fluid
- C : sound speed in fluid

In the acrylic cylinder test, the gas work of the 3 g charge for 40 MPa was approximately 1 kcal as shown in Figure 6. The PI values of different charges, that are estimated by using the coefficient  $4\pi R^2 / \rho C$  obtained when the PI value is assumed to be the same as gas work for 40 MPa, coincide well with the other gas works as shown in Table 1. Therefore according to the pressure history  $P(t)$  measured actually near the source, the energetics level of the source for 60 MPa is expected to be approximately 2 kcal.

## 4. TEST RESULTS AND DISCUSSION

### 4.1. Comparison with rigid vessel

A rigid vessel is used to measure pressure propagation without interaction. Figures 7-A to 7-C show comparison between the pressure history, strain history and deformation profile with respect to a rigid vessel and capsules with different shell thicknesses when identical sources for 40 MPa were used.

The pressure waves repeat reflection between the free surface acting as an upper boundary and the rigid surface acting as a lower boundary. After the pressure wave in fluid dissipated, the slug gained kinetic energy and impacted against the plug, thus terminating the phenomenon.

As shown in Figure 7-A, rigid wall reflection which was double the initial peak pressure near the source ( $P_2$ ) was generated at the bottom ( $P_4$ ) of the capsule. Its duration was about 275  $\mu$ s (dividing the depth of water, 400 mm, by sound velocity, 1,450 m/s) in which rarefaction that started from the free surface reached the bottom of the capsule. The reproducibility of the pressure history in a rigid vessel was  $\pm 10\%$ .

In cases where a capsule is deformed, rarefaction due to the deformation of the source part of a capsule was also propagated to the bottom of a capsule. So the initial waves are broken up into several parts ( $\text{\textcircled{a}}$  in Figures 7-B and 7-C), and the initial peak pressure becomes lower in comparison with the case of a rigid vessel. Therefore pressure waves propagated to and reflected from the bottom cannot be regarded as the original to predict the source level when the source part is deformed. Pressure history near the source was not measured in case of the deformable capsules.

A thinner capsule (thickness ( $t$ ): 2 mm) permitted higher deformation of the source part of a capsule and further lowered the initial peak pressure at the bottom as shown in Figure 7-C. Nevertheless, the lower part of the capsule is deformed more severely because it is thinner than  $t = 3$  mm. The pressure waves tended to break up and dissipated more easily.

As the deformation of the source part of a capsule increased, the slug movement velocity also dropped, thus lowering the slug impact pressure and delaying the time of its occurrence. (Compare the pressure histories of  $P_6$  in Figures 7-A to 7-C.) By dividing the initial peak pressure  $P_6$  in Figure 7-C by  $\rho C$ , the movement velocity at the time of slug impact is estimated to be 80 to 90 m/s. The circumferential strain ( $S_{17}$ ) at the lower part of the capsule shown in Figure 7-C did not settle but decreased gradually due to the spring back effect of the rigid part of the bottom of a capsule.

The important point in design of such types of capsules to avoid deformation localization is to absorb strain within the allowable plastic range in the vicinity of the source part, thus preventing pressure waves from building up in the upper and the lower part of capsules.

#### 4.2. Absorbed strain energy

Based on circumferential strain ( $\epsilon_\theta$ ) and axial strain ( $\epsilon_l$ ), " $\epsilon_\theta + \epsilon_l + \epsilon_r = 0$ " was used to find the radial strain ( $\epsilon_r$ ), and the strain energy that a capsule absorbed was calculated in order using the equivalent plastic strain  $\epsilon_{eq}$ . The strain rate exceeded  $200 \text{ sec}^{-1}$  at each location of deformation, but the dependency was neglected and the strain rate  $\dot{\epsilon} = 2 \text{ sec}^{-1}$  was used uniformly here. So the precise strain energy will be corrected later when sufficient dynamic material data are collected.

The strain energy of the capsule is divided into the source part and the lower part as indicated by the deformation profile. In the examples of Figures 7-B and 7-C, the total strain energy applied to a capsule of  $t = 3 \text{ mm}$  and  $2 \text{ mm}$  are about 150 and 780 cal, respectively. So the strain energy changes according to the strain absorbing ability of a capsule structure, and thus the conversion ratio cannot be constant. In other words, the distribution ratio of the released energy converted into the internal energy, kinetic energy and strain energy depend on the strain absorbing ability.

Figure 8 shows the correlation between strain energy and strain absorbing ability which was assumed to be a function of  $PI/t$  ( $t$ : thickness). The source part of a capsule is as curved as the stress-strain relationship and starts from the  $PI/t$  value corresponding to the yield point (Figure 8-  $\odot$ ). The strain energy of the lower part, on the contrary, tended to be constant as against  $PI/t$  due to the end effect of the capsule (Figure 8-  $\triangle$ ). When the  $PI/t$  value increased, the capsule deformation mode changed in the order of alphabetic  $b \rightarrow B \rightarrow D$  (Yoshie and Saito 1987), and the source part deformation would exceed lower part deformation, namely, the mode of the source part would be maximum.

### 5. CONCLUSIONS

- (1) As a result of a comparison with the released energy measured by directly visualizing the gas expansion, it is suggested that the energetic level can be predicted by the  $PI$  value computed by using the pressure history near the source in a rigid case.
- (2) In cases where the capsule source part is deformed, resultant pressure waves at the bottom of a capsule break up, and initial peak pressure is lowered. Similarly, slug impact pressure drops, and as a whole, localization of deformation tends to be prevented.
- (3) The conversion ratio for changing to the strain energy differs according to the strain absorbing ability of a capsule structure. In this report, the strain ability is represented by  $PI/t$ , and thus the correlation with the strain energy has been clarified.

### REFERENCES

- Tanzawa, S., et al. (1989) The previous paper: Shock Structural Tests for NSRR Experimental Capsule Using Slow Explosive, 10th SMiRT, Anaheim
- Cole, R.H., (1965) On the Theory of the Shock Wave: Underwater Explosions pp.110 – 146
- Yoshie, S., Saito, M., (1987) Four Deformation Profile Types: Shock Structural Response of Reactor Vessel under HCDA in LMFBR, 9th SMiRT, Lausanne.

**Table 1 Gas work & PI value**

Explosive charge Z [g]	Peak pressure near source P <sub>p</sub> [MPa]	Impulse of P(t) I [KPa·s]	PI [cal]	Gas work until cover-gas W = ∫ p dV [cal]	Slug velocity at impact v [m/s]
0.75	11	7	120*	130**	38
0.90	13	9	180*	190**	49
1.05	16	9	230*	220**	52
1.35	20	12	380*	270**	62
3.00	40	16	1000	1000***	82

Notes \* ; PI was calculated with  $4\pi R^2 \rho C$  obtained from the gas work W of 3.0 g charge.  
 \*\* ; Float was used for measuring the gas expansion.  
 \*\*\* ; Gas expansion was directly measured through acrylic tube.

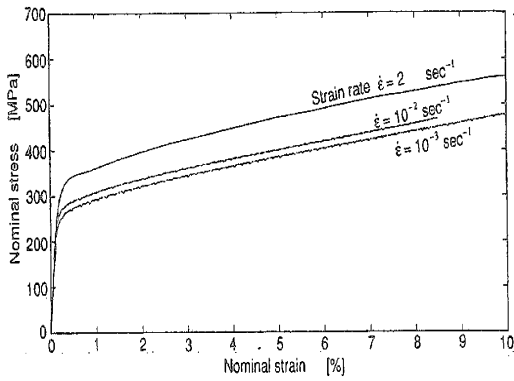


**Fig. 2 Stress-strain curve of capsule material**

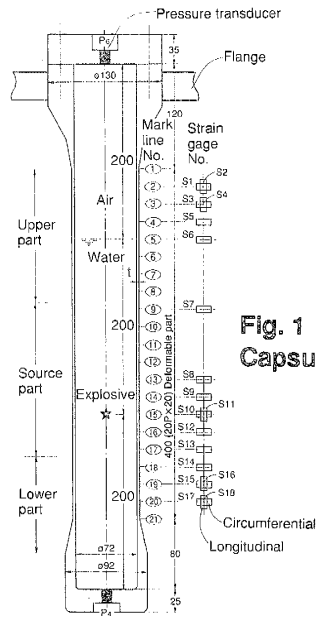


**Fig. 1 Capsule model**

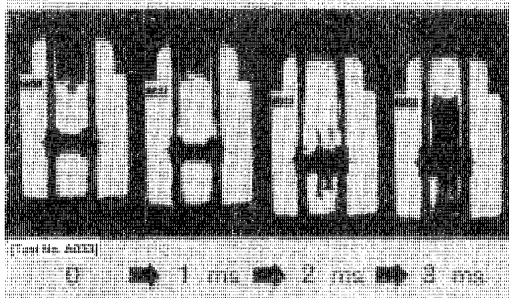


**Fig. 4 High speed photograph of gas expansion**

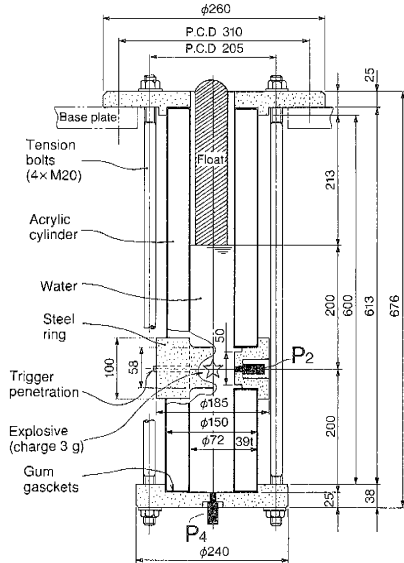


**Fig. 3 Acrylic cylinder for gas expansion**

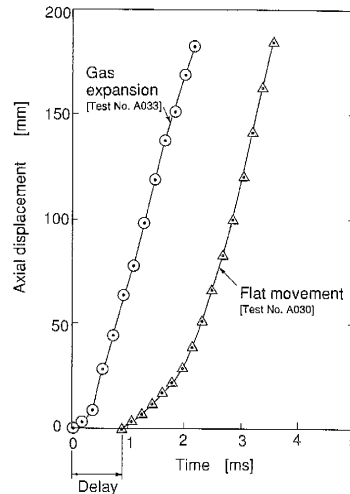


**Fig. 5 Gas expansion & float movement**

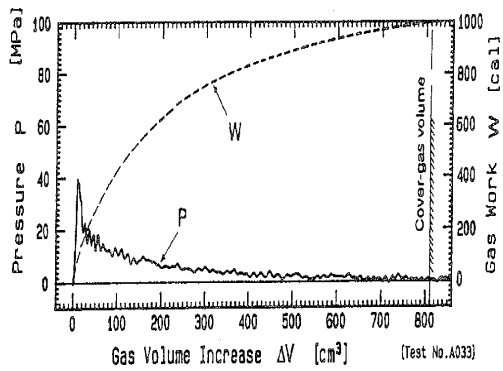


Fig. 6 Pressure- & gas work- volume change relationships for energy source

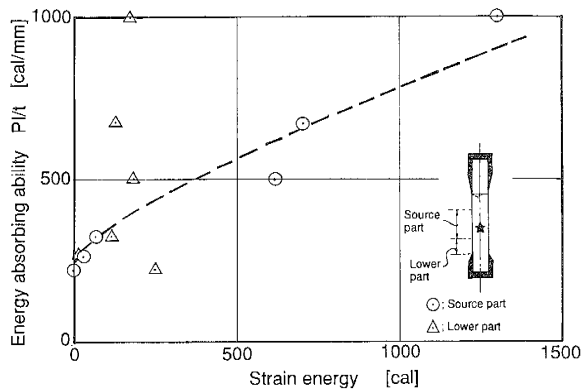


Fig. 8 Strain energy v.s. energy absorbing ability

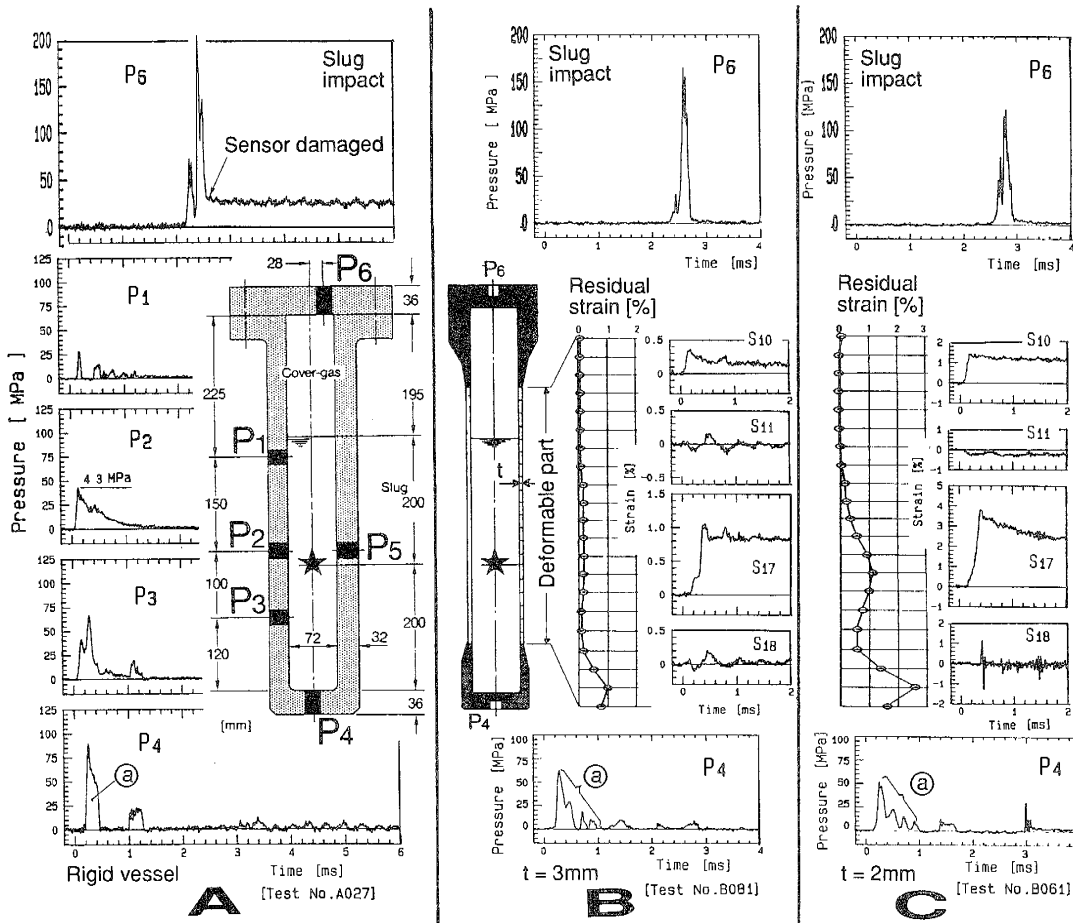


Fig. 7 Comparison of pressure & strain history (charge: 3 g)